Fermi-level pinning can determine polarity in semiconductor nanorods

Philip W. Avraam, Nicholas D. M. Hine, Paul Tangney, and Peter D. Haynes*
Department of Physics and Department of Materials, Imperial College London, Exhibition Road, London SW7 2AZ, United Kingdom
(Received 28 October 2011; published 5 March 2012)

First-principles calculations of polar semiconductor nanorods reveal that their dipole moments are strongly influenced by Fermi-level pinning. The Fermi level for an isolated nanorod is found to coincide with a significant density of electronic surface states at the end surfaces, which are either mid-gap states or band-edge states. These states pin the Fermi level, and therefore fix the potential difference across the rod. We provide evidence that this effect can have a determining influence on the polarity of nanorods, with consequences for the way a rod responds to changes in its surface chemistry, the scaling of its dipole moment with its size, and the dependence of polarity on its composition.

DOI: 10.1103/PhysRevB.85.115404 PACS number(s): 73.22.−f, 61.46.Hk

I. INTRODUCTION

Semiconductor nanostructures in solution are a very exciting class of material due to our growing ability to manipulate their shapes and sizes, and the superstructures into which they assemble, to produce a wide range of technologically useful properties.[1–7]

Nanocrystals of binary semiconductors, such as those of ZnO, have been observed to exhibit very large dipole moments[8–10] which affect their internal electronic structure (and therefore their optical properties) as well as their interactions with their environment. The latter may influence the kinetics of self-assembly and the stability of the structures formed.[11]

A detailed understanding of the factors contributing to this polarity in nanocrystals has proven elusive[12] for two main reasons. First, many factors are involved, ranging from surface chemistry, to the noncentrosymmetric nature of the underlying crystal, to quantum confinement, to long-range electrostatics, to interactions with the solvent and considerations of thermodynamic stability. Second, the limitations of current experimental techniques do not allow the level of control over, or knowledge of, the state of the system, which is necessary to be able to disaggregate these factors.

Computer simulation is an ideal tool for addressing these problems.[13–16] Recent developments in linear-scaling density-functional theory (LS-DFT), make accurate quantum-mechanical methods applicable to nanocrystals of realistic sizes.

In our earlier work[17] we presented results from LS-DFT calculations using the ONETEP code[18,19] of the ground-state charge distributions in GaAs nanorods of sizes comparable to those found in experiments. We found that the nanorod dipole moment depends strongly on the surface termination, particularly of its polar surfaces, with full hydrogen termination on polar surfaces strongly reversing its direction.

A common feature of all of the nanorods studied was that the Fermi energy was found to coincide with a significant density of states located at the end surfaces of the rods. *Fermi-level pinning* (FLP) is known to occur in semi-infinite semiconductor surfaces when states are found at the Fermi energy, and in this work we show that a finite-surface version of FLP plays a crucial role in determining the polar characteristics of such nanorods.

In Sec. II we outline the simulation details and methodology. In Sec. III we show that mid-gap states on the end surfaces of the rod can pin the Fermi energy, which in turn determines the potential difference across the nanorod, and therefore its dipole moment.

In Sec. IV we take up an important observation from our previous work, namely that nanorods terminated on their ends with ions of very different ionic charge can nevertheless have very similar dipole moments. This observation is particularly problematic for simple ionic or bond-electron counting models,[12] which can fail to predict the dipole moments as a result. These models are not able to explain the magnitudes of the differences in polarity between nanorods of different surface terminations. We show that our FLP model can rationalize these observations.

In Sec. V we calculate the variation of nanorod polarization with rod length and cross-sectional area. The dipole moment is found to increase with nanorod size in a manner consistent with maintaining a "pinned" Fermi level at the end polar surfaces of the nanorod.

Finally, in Sec. VI we study the variation in polarity between nanorods of different compositions (specifically GaAs, GaN, and AlN), again illustrating the determining role of FLP for the rod polarizations.

II. SIMULATION METHODOLOGY

This work uses linear-scaling density-functional theory (LS-DFT) as implemented in the ONETEP code.[18,19] This method combines the benefits of linear scaling, in that computational resources for calculating the total energy of an N-atom system scales as $O(N)$, with the accuracy of plane-wave methods.[20] In ONETEP the single-particle density matrix is represented by an optimized set of nonorthogonal, strictly localized, Wannier-like orbitals $\{\phi_\alpha(\mathbf{r})\}$, and is written

$$\rho(\mathbf{r},\mathbf{r}') = \sum_{\alpha\beta} \phi_\alpha(\mathbf{r}) K^{\alpha\beta} \phi^*_\beta(\mathbf{r}'), \tag{1}$$

where $K^{\alpha\beta}$ is the *density kernel* representing a generalization of the occupation numbers to a nonorthogonal basis. Both the local orbitals and the density kernel are optimized during the calculation. The three tuneable parameters controlling the quality of the representation are[21] the "plane-wave" cutoff

energy E_{cut}, defining the grid-spacing for the grid on which the local-orbitals are represented; the local-orbital cutoff radius R_ϕ for each atomic species; and the density kernel cutoff radius R_K.

Exchange and correlation is treated within the local density approximation (LDA). Errors resulting from the supercell approximation, which can be large in systems with a monopole or a strong dipole, are eliminated using a truncated Coulomb potential.[22,23] Basis-set superposition error that could affect the treatment, within a local-orbital framework, of surface adsorption is eliminated by the optimization procedure.[24]

A further advantage of our method over other computational methods that have been used to study nanocrystals[16] is that the whole of the nanostructure is included in the calculation in a way that allows the electrons throughout the nanostructure to reach a global equilibrium. We are therefore able to accurately account for any coupling that may (and in fact does, as we shall show) occur between different regions of the nanostructure. We caution that this method presupposes integer occupations, which precludes partial occupancies of states that might otherwise occur in a traditional calculation where the system is treated as metallic. We have also performed test calculations which permit fractional occupancies (albeit with cubic-scaling computational cost) on representative smaller systems, which confirm that the states presented here are indeed lowest in energy.

Primarily, we study nanorods of wurtzite GaAs (though we also model GaN and AlN), since it exhibits all of the important characteristics of a polar semiconductor, i.e., elements of both ionic and covalent bonding character and a noncentrosymmetric lattice structure. Ion cores are represented using norm-conserving pseudopotentials. It has been shown in previous work[25] that an adequate description of the geometry of systems containing Ga requires either the explicit inclusion of the Ga $3d$ electrons in the calculation, or, if the $3d$ electrons are frozen into the pseudopotential, nonlinear core corrections[26] should be applied. To reduce the computational cost, we have chosen the latter approach for both the Ga and As pseudopotentials.

An effectively infinite kernel cutoff radius R_K was used in order to treat insulators and metals on an equal footing. Calculations using plane-wave DFT, as implemented in the CASTEP code,[27] show that setting $E_{\text{cut}} = 400$ eV is sufficient to converge bond lengths, bond angles, and total energies of bulk GaAs, Ga_2, and As_2 dimers to within 0.02% of their 800 eV values, using our pseudopotentials. We find that bond lengths are underestimated by 1.3%, which is typical for LDA. ONETEP is known to require a 10%–20% larger E_{cut} than CASTEP for the same level of convergence,[19] thus, the calculations in this work use $E_{\text{cut}} = 480$ eV and a generous local orbital radius of $R_\phi = 0.53$ nm.

For analysis of the dipole moment, we calculate the quantity $\mathbf{d} = -\int n(\mathbf{r})\mathbf{r}\,d\mathbf{r} + \sum_I Z_I \mathbf{R}_I$ from the density $n(\mathbf{r})$ in the whole simulation cell, and the positions $\mathbf{R}_I$ of the ions of charge Z_I. The internal electric field is calculated from the gradient of the value of the local effective potential smoothed over a volume equivalent to one primitive cell of the underlying material, as in our previous work.[17]

III. FERMI-LEVEL PINNING IN NANORODS

We first consider the ground-state electronic structure of a structurally relaxed nanorod of length 12.8 nm and cross-sectional area 3.56 nm^2, comprising 2862 atoms. The rod (represented schematically in Fig. 1) is labeled H/H-r, where the first three symbols (H/H) denote that the lateral/end surfaces are terminated with hydrogen atoms, and "-r" denotes that it is structurally relaxed.

This rod has a large negative dipole moment of −600 D and a large internal field of +0.1 V/nm in the center of the rod. We adopt the convention that a negative dipole moment is one whose direction opposes that of the spontaneous polarization of the underlying wurtzite crystal lattice (the wurtzite [0001] direction, which is referred to as the z direction in this work). In Fig. 1 we plot the "slab-wise" local density of electronic energy states (LDOS) for this rod. We define a slab LDOS as follows: the rod is nominally divided into 20 slabs along its length (the z direction), each consisting of four planes of atoms: two each of Ga and As. The slab LDOS is the sum of the contributions to the total DOS from the local orbitals centered on those atoms. In Fig. 1 we superpose these slab LDOS. It is clear that the electric field shifts the individual slab LDOS with respect to one another.

The Fermi energy can thus be considered to coincide with a significant density of states on both polar surfaces of the nanorod. On the Ga(-H) polar surface these states are mid-gap states, and on the As(-H) surface, these mid-gap surface states are adjacent to the conduction band edge. These are very stable positions for the Fermi level because small deviations

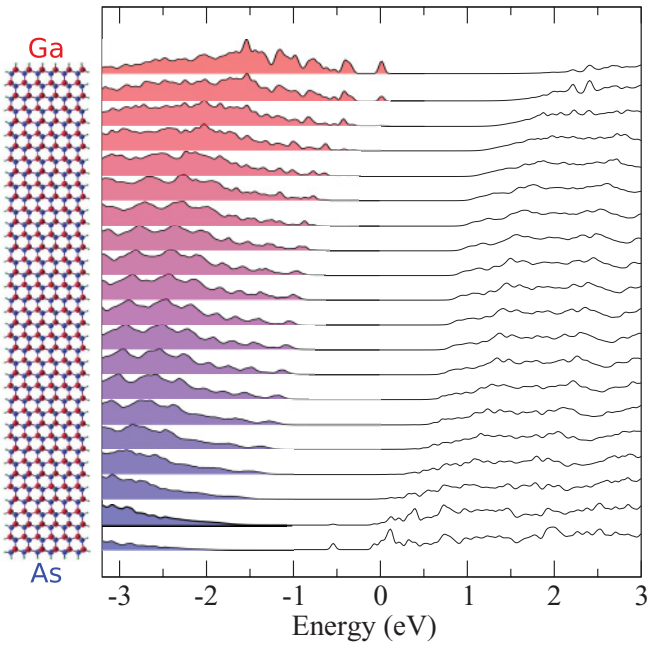

FIG. 1. (Color online) Structurally relaxed, fully hydrogen terminated GaAs nanorod (left) and the LDOS (right) for each slab, consisting of four planes of atoms (two As and two Ga). The filled curves indicate the occupied (valence) states at each slab. The band-edge states at opposite ends of the rod are seen to coincide in energy.

from these positions would cause changes in occupancy of the surface states, resulting in a redistribution of charge and a potential opposing the redistribution. This is analogous to Fermi-level pinning exhibited by some semiconductor surfaces, in which a group of mid-gap states fixes the Fermi level at the surface at the position of their average energy due to the action of surface states as donors or acceptors, which get filled or emptied to compensate for any change that may affect the relative position of the Fermi level (e.g., the application of a voltage). We see this principle in action in Fig. 1, in that any significant occupancy of the lowest-energy empty state on the As(-H) surface (which appears to lie below the Fermi level) would in fact bring it above the Fermi level due to the change in the electric field produced by the charge redistribution. Of course, although this filling and emptying of states can occur unaided in a DFT calculation, it would, in real systems, depend on the availability of free charges in the environment, implying an important role for the solvent.

There are at least two important differences between FLP on semi-infinite surfaces and the finite end surfaces of nanorods. First, on surfaces of area A, changes in surface charge density $\Delta\sigma$ due to changes in occupancy of surface states come in discrete amounts (i.e., $\Delta\sigma = e/A$), meaning that the continuous variability of the surface charge density on semi-infinite surfaces gives way to a discrete variability on finite surfaces. Second, the analog of the *depletion region* associated with FLP is the charged region on the opposite end of the nanorod, meaning that the two surfaces are coupled. This second effect may confer an important role on the environment surrounding the nanorod, which may mediate the interaction between the coupled ends by facilitating the transfer of electrons between them as the system is perturbed.

In our previous work,[17] we studied rods with a range of different polar surface terminations, and with dipole moments ranging from $+330$ to -614 D. In all cases, the nanorods exhibited this same feature of having Fermi levels coinciding with the energies of large densities of mid-gap states on the end polar surfaces of the nanorods. The arguments made here about FLP apply to all nanorods with this feature.

One immediately obvious consequence of this picture is that the dipole moment and internal field of a nanorod are dependent on the energies of the pinning states on both ends of the rod, relative to their local (slab) band edges. The difference between these relative energies defines how much the energy spectrum is shifted between the top and bottom ends of the nanorod, i.e., the potential difference ΔV between the ends. If the Fermi level is pinned on both ends of the rod, then the potential difference ΔV must also be pinned. We will find, in each of the subsequent sections in this work, that this pinning of ΔV plays a crucial role in determining the polarity of a nanorod.

The pinning states in rod H/H-r on both ends of the rod are mid-gap states, though they are adjacent to the band edges in this case. Different surface reconstructions on the polar surfaces may remove these mid-gap states or change their positions relative to the local energy spectra. This could change the potential difference across the rod and, therefore, the dipole moment.

IV. EFFECT OF SURFACE CHEMISTRY ON DIPOLE MOMENT

Another implication of the picture presented above is that it is overly simplistic to cast the problem of nanorod polarity in terms of an ionic model, or a simple bond-electron counting model, since these models do not include constraints on the potential difference across a nanorod imposed by FLP. In previous work,[17] we found that the dipole moment d_z, the charge on the bottom (As-rich) end Q_b, and the electric field in the middle of the rod E_m for two unrelaxed nanorods (labeled H/H and H/P) were all very similar, despite having surface terminating species of very different ionic charge. Rod H/H is fully hydrogen terminated on both the lateral ($\parallel$ to z) surfaces and the polar ($\perp$ to z) surfaces. Rod H/P, on the other hand, is terminated with hydrogen atoms on the lateral surfaces, while on the polar surfaces there are pseudohydrogen[28] atoms of two different varieties. These pseudohydrogen atoms are used to passivate the dangling bonds of their respective surfaces: those on the Ga polar surface have an ionic charge of $+1.25e$, while those used to terminate the As polar surface have an ionic charge of $+0.75e$. These pseudoatoms are intended to passivate dangling bonds on the polar surfaces, without adding charge to them, and they have been shown in other work to render the surfaces electronically inert.[28]

A simple bond-electron and ion counting argument predicts that the Ga polar surface on H/P should have an additional charge of $+0.25e$ for each of the 27 bound pseudoatoms, compared to H/H—a total change of $+6.75e$ for each end. Similarly, the As polar surface should have a reduced charge of $-0.25e$ per pseudoatom—a total change of $-6.75e$. Nanorod H/P should therefore have a greatly reduced dipole moment and potential difference across it. In fact, we observed d_z, Q_b, and E_m change from -614 D, $1.00e$, and 0.100 V/nm respectively in H/H, to -531 D, $0.95e$, and 0.105 V/nm in H/P—a much smaller change.

We plot the electron density difference between rods H/H and H/P in Fig. 2. The densities have been integrated in the x and y directions and convolved with a Gaussian of standard deviation 0.32 nm in the z direction. The latter process smooths out variations on length scales smaller than a unit cell length. By integrating the resulting curve from each end to the center of the rod, we find that there has been a transfer of 6.70 electrons from one end of the rod to the other between rods H/H and H/P, which almost entirely cancels the change in ionic charge. In Fig. 3, we plot the LDOS of only the top (the Ga-rich polar end surface) and bottom (the As-rich polar end surface) slabs of both rods H/H and H/P. By summing the occupations of the states plotted in this figure, we find that there has been a change of 6 in the number of occupied states on each end of the rod between H/H and H/P. The remaining charge transfer of $0.70e$ must be associated with the polarization of occupied states in slabs far away from the ends. This polarization of the electron density can be observed in the inset to Fig. 2. The potential difference between the ends ΔV is very similar for both rods: 1.8 eV for H/H and 1.5 eV for H/P.

It is instructive to consider a fictitious adiabatic process in which the ionic charge of the polar terminating species is slowly tuned so as to go from rod H/P to H/H. The LDOS on the rod ends begins with the Fermi level at the local band

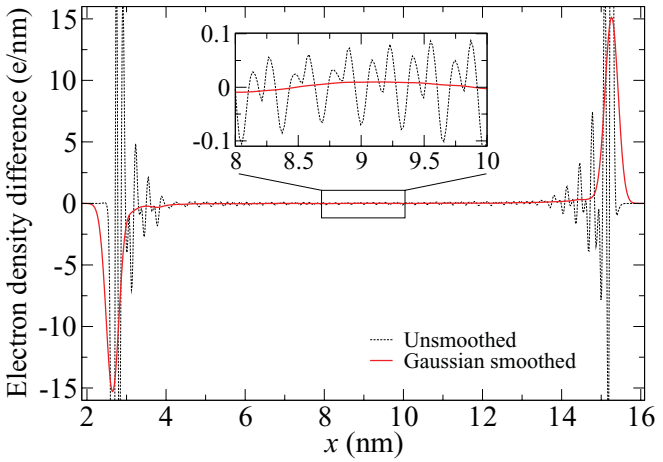

FIG. 2. (Color online) The difference in laterally integrated electron density profiles between H/H and H/P. The standard deviation of the Gaussian used to smooth the data parallel to the nanorod axis is 0.32 nm. There has been a shift of 6.70 electrons from left to right. We show that the majority of this redistribution is attributable to changes in surface state occupancy.

edge on each end of the rod, adjacent to the electronic states. Therefore, we have $\Delta V \approx E_g$ in this case. As the charges of the terminating pseudoatoms decrease on the Ga end, and increase on the As end, the energy of nearby electronic states on the Ga end of the rod must increase, pulling some of those that lay just below the Fermi level, above it, and vice versa on the As end. This causes these states to change occupancy and compensate some of the change in ionic charge. The higher the density of states at the Fermi level, the less mobile is the Fermi level (i.e., the more strongly the Fermi level is pinned). To effect a given shift in the Fermi level, a larger change in surface ionic charge is required if the density of states is high. That is to say, energies coinciding with a high density of states (such as the band edges) represent regions of high stability for the Fermi level. The transition from H/P to H/H causes the Fermi energy to run in to the (local) band edges, which is

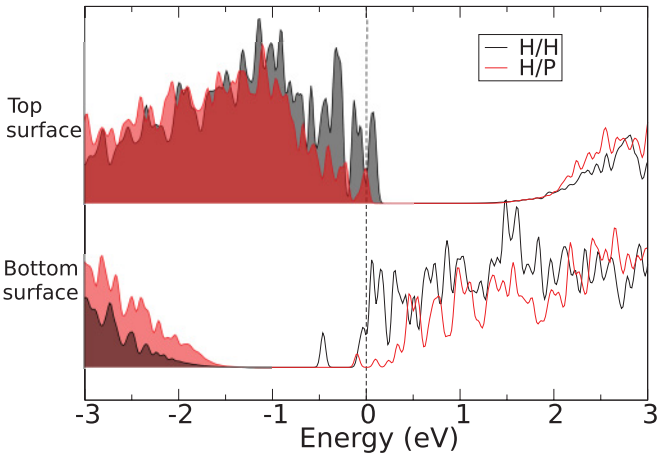

FIG. 3. (Color online) Local densities of states for the slab of atoms on the Ga-rich (top) and As-rich (bottom) ends of nanorods H/H and H/P. The potential difference between the two ends $\Delta V \sim 1.8$ eV for H/H and 1.5 eV for H/P.

why there is very little change in the pinned position of the Fermi level on both ends, and therefore very little change in the potential difference ΔV between the ends of the rod.

The general conclusion from this section is that changes in nanorod polarity due to changes in ionic charge at the surfaces of nanorods can be screened out due to FLP occurring at the ends of the nanorod. This effect tends to preserve the potential difference between the ends of the nanorod, ΔV, and consequently, the dipole moment. The band-gap E_g, in effect, imposes an approximate upper limit on ΔV, since the density of states within the bands is so high that the Fermi level would be very strongly pinned at its edges.

V. EFFECT OF LENGTH AND CROSS-SECTIONAL AREA ON DIPOLE MOMENT

In this section, we look at how the dipole moment of nanorod H/H varies with rod length L, and cross-sectional area A, and show how it can be explained using our FLP model.

We find, from Fig. 4, that the dipole moment increases roughly linearly with L over the range studied, for rods of $A = 3.56$ nm^2. This implies that the excess polar surface ground-state charge density on each end surface is independent of nanorod length over this range.

In Fig. 5 we show how both the dipole moment and the polar surface charge *density* σ on the bottom (As) end surface of the rod change with A for a fixed nanorod length of $L = 12.8$ nm. The charge density σ on the polar end surfaces decreases rapidly with cross-sectional area, asymptotically approaching a constant value that may well be slightly above zero for nanorods of this length (because surfaces of polar thin films, unlike semi-infinite surfaces, can support a nonzero charge[12]).

We turn to consider the causes of these scaling relationships, focusing first on the variation in rod polarization with respect to A. The slab-LDOS plots in Fig. 6 show that, for all of the cross-sectional areas studied, the occupied states on the top surface align closely with the unoccupied conduction band edge on the bottom surface. In the previous section we argued that the local band edges represented an effective upper and lower limit for the Fermi energy on the ends of a nanorod, and

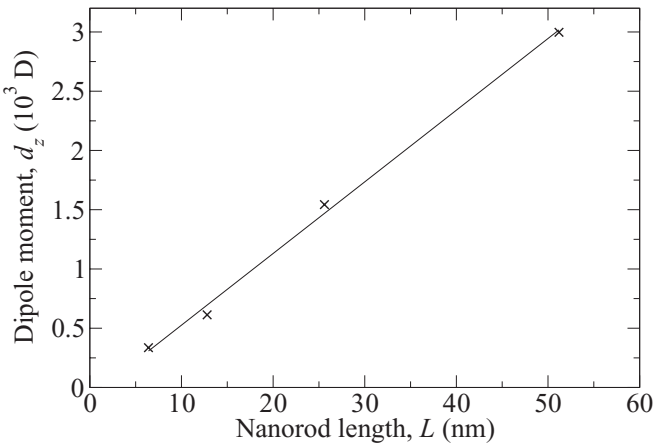

FIG. 4. The magnitude of the dipole moment increases linearly with nanorod length for nanorods of cross-sectional area $A = 3.56$ nm^2.

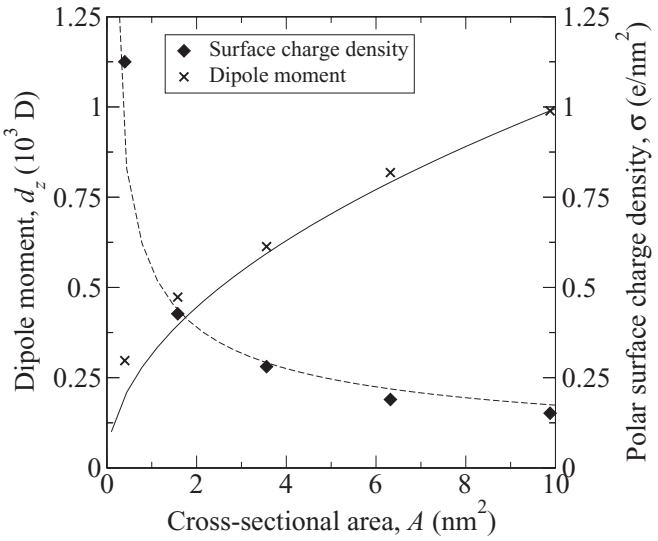

FIG. 5. The magnitude of the dipole moment increases with nanorod cross sectional areas for nanorods of length $L = 12.8$ nm. Curves are fitted to the data, with functional forms $\sigma(A) = c_1/(\sqrt{A} + c_2 - \sqrt{A + c_2^2})$ and $d_z = c_3 A/(\sqrt{A} + c_2 - \sqrt{A + c_2^2})$, derived from Eq. (3). Over this range $\sqrt{A} \ll c_2$, placing these rods firmly in the "thin" regime.

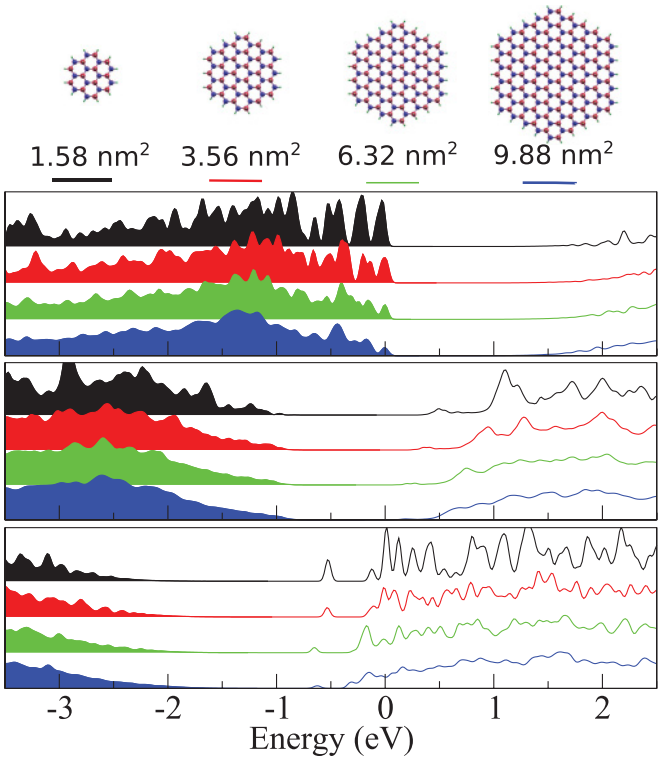

FIG. 6. (Color online) Slab-wise local densities of states for rods of four different cross-sectional areas, sampled at three positions on the rod: (top) the slab on the Ga-rich end, (middle) the slab in the middle of the rod, and (bottom) the slab on the As-rich end. For ease of comparison, we have shifted the energy of the highest occupied state for each rod to zero. The Fermi level can be imagined to remain adjacent to the band edges for all rods, and the band-gap is larger for thinner rods due to quantum confinement.

that the polarization of rod H/H, in particular, is constrained by these band edges (evidenced by the fact that going from H/P to H/H does not change the dipole moment very much, because the Fermi level touches the band edges at both ends of the rod).

In such a rod, the potential difference between its ends, ΔV, is determined mostly by its band-gap E_g, so that $\Delta V \approx E_g$. We will argue that this observation alone can qualitatively account for the observed trends in d_z and σ with A in Fig. 5. While we do not expect the band gap of equivalent real nanostructures to match exactly with the DFT gaps we observe (due to the well-known band-gap error of DFT), we expect qualitatively the same behavior to emerge.

We can analyze this behavior in terms of a simple electrostatic model, and compare this to the results in Fig. 5. The electrostatic potential due to a circular disk of radius a and area charge density σ at a distance z along its axis is given by

$$V(z) = 2\pi\sigma(\sqrt{a^2 + z^2} - |z|). \tag{2}$$

This expression simplifies to the familiar results for a point charge in the limit that $z \gg a$ and infinite slab when $z \ll a$. Assuming equal and opposite densities at the two ends of the rod, $z = 0$ and $z = L$, the total potential difference is $\Delta V = 2[V(0) - V(L)]$ ($\approx E_g$ in this case), which rearranges to give

$$\sigma \approx \frac{E_g}{4\pi(a + L - \sqrt{a^2 + L^2})}. \tag{3}$$

For "thick" rods, $a \gg L$, $\sigma \sim E_g/L$, independent of a to leading order, whereas for "thin" rods, $a \ll L$, $\sigma \sim E_g/a \propto E_g/\sqrt{A}$. The rod dipole moment $d_z = \sigma AL$ therefore scales as $d_z \sim E_g A$ for thick rods but as $d_z \sim E_g \sqrt{A} L$ for thin rods. Substituting $a \propto \sqrt{A}$ into Eq. (3) yields a general expression for $\sigma(A)$, which we fit to the data in Fig. 5. We also fit the curve given by the expression $d_z = \sigma AL$ to the data for d_z.

Evidence of deviation between our model and the data can be seen at smaller values of A in the data for d_z. The smaller A is, the larger the error in our model. This is not surprising because the model assumes that charge is localized on planes at the ends of the rod, but we know that as A becomes smaller, the surface charge becomes increasingly delocalized along z. Furthermore, at small A the rod cross section is increasingly dominated by edge atoms rather than atoms truly belonging to the polar surface. For these reasons, a breakdown of the model is expected at very small values of A. Despite this complication it is clear from the fitting parameters that our rods are in the thin regime, as defined above, as the model form correlates well with the observed behavior. In summary, thinner nanorods exhibit stronger decay of their internal potential, due to finite width effects, therefore thinner rods require a larger charge density on the nanorod ends, in order to generate the required potential difference ΔV, than do thicker rods.

There is a second and less significant feature in the LDOS plots of Fig. 6, that serves slightly to complicate the picture described above. From the data sets in the middle panel of Fig. 6, thinner nanorods are found to exhibit a larger local band gap than thicker rods. The local band gap in the middle of the rod is found to be 1.3 eV in the thinnest rod, and 0.9 eV in the thickest. This is due to quantum confinement of electronic states in the lateral direction, which is stronger in thinner rods.

As the band gap increases, the potential difference between the ends of the rod can increase, which further increases the amount of charge density required on the end surfaces of the thinner nanorods in order to meet the resulting increased pinned potential difference.

Although both of these effects (i.e., loss of the internal field due to finite-size effects, and the increase in the band gap due to quantum confinement) play a role in generating the behavior seen in Fig. 5, the first is more significant, since quantum confinement produces only a 44% increase in the band gap over the range of rods studied, which does not come close to accounting for the 740% increase in the polar surface charge density over the same range.

We return now to the variation in nanorod polarization with L. We did not observe quantum-confinement-related variation as was observed over the range of A. Presumably, this is due to the large extent of the rods in the z direction. However, just like over the range of A, we found that the Fermi level remains pinned close to the band edges over the range of L, resulting in the potential difference between the nanorod ends remaining constant.

The rods in Fig. 4 are able to maintain the charge on their ends as L increases, without incurring a significant change in the potential difference across the rod, because the rod is very thin, and the internal potential decays very strongly: the fields in the middle of rods of length 12.8, 25.6, and 51.2 nm are found to decay to values of 0.1, 0.035, and 0.009 V/nm respectively in the rod centers. If the rods were thicker, we would expect this decay to be weaker, and the amount of charge on the ends to be reduced with L to maintain the pinned potential difference, thus reducing the rate at which the dipole moment increases with length.

In summary, FLP plays a determining role in the scaling of the dipole moment of the nanorods studied, with length and cross-sectional area. This effect manifests itself in different scaling behavior, the details of which depend primarily on the rate of decay of the internal electric field (which is a function of A), the length L of the rods, and the pinned potential difference ΔV, which is close to the size of the band gap for rods in which the Fermi level is pinned near the local band edges, as is the case in the particular rods studied in this section. Quantum confinement may also have some influence on this scaling by affecting ΔV.

VI. EFFECT OF NANOROD COMPOSITION

In this section we investigate how the polar behavior of nanorods depends on composition. We calculate the charge distribution in three rods: one composed of GaAs, another of GaN, and a third of AlN. These are all III-V semiconductors, so their chemistry and response to terminating ligands can be expected to be similar. We therefore terminate the rods with the same atoms as in previous sections, as type H/P (lateral surfaces fully covered with hydrogen atoms, and polar surfaces fully covered with the appropriate passivating pseudohydrogen atoms). All have the same number of atoms (2862), and are constructed of the same number of unit cells in each direction. Atoms are located at their bulk equilibrium values, as calculated in the CASTEP plane-wave-DFT code, meaning that the GaAs rod is longer than the GaN rod, which in turn is longer than the AlN rod, because of the differences in bulk lattice parameters.

TABLE I. Some properties of AlN, GaN, and GaAs in nanorod and in bulk. Experimental data for AlN were obtained from Refs. 29–31, for GaN from Refs. 32–34, and for GaAs from Refs. 35,36.

	AlN	GaN	GaAs
	Bulk		
DFT lattice param a (Å)	3.075	3.154	3.935
DFT lattice param c (Å)	4.941	5.132	6.486
DFT polarization (C/m^2)	0.073	0.029	0.005
DFT (LDA) bandgap (eV)	4.5	2.7	0.9
Experimental bandgap (eV)	6.2	3.3	1.5
Experimental permittivity, ϵ_r	8.5	9.7	13.1
	Rod		
Length L (nm)	9.66	10.01	12.61
Cross-sectional area A (nm^2)	2.26	2.33	3.62
d_z (D)	−713	−682	−531
Polarization (C/m^2)	−0.11	−0.098	−0.039
ΔV (eV)	4.2	3.2	1.5
Q_b (e)	1.61	1.50	0.95
σ_b (e/nm^2)	0.711	0.645	0.262
Q_b decay constant (nm^{-1})	1.02	0.80	0.48

The main characteristics of these rods and their charge distributions are summarized in Table I, along with reference information about the bulk properties of these semiconductors.

Figure 7 shows the distributions of charge along the lengths of the rods for the three nanorods, integrated in the x and y directions and in the z direction, convolved with a Gaussian of standard deviation $c/2$ so as to smooth out variations on length scales smaller than the length of half a unit cell length c (N.B., c is different for each of the rods, as summarized in Table I).

In Fig. 8 we plot the LDOS for the polar surfaces of the three rods. In all cases, the Fermi level can be imagined as being pinned by surface states near the band edges, for reasons outlined in previous sections.

The polarization of the rod appears to increase proportionally with the potential difference across the rod, ΔV,

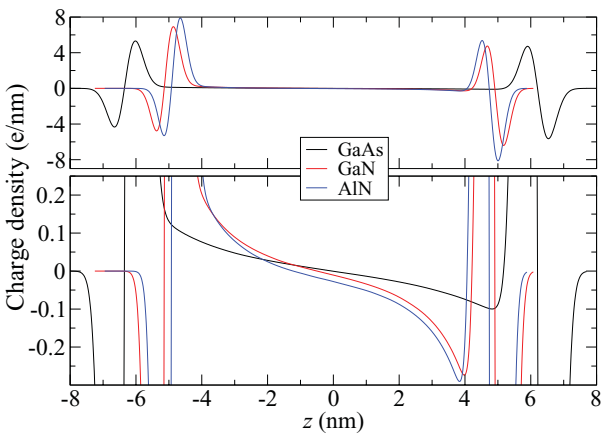

FIG. 7. (Color online) Laterally averaged and Gaussian-smoothed charge distributions along the lengths of nanorods of AlN, GaN, and GaAs. The ordinate has been magnified in the lower panel.

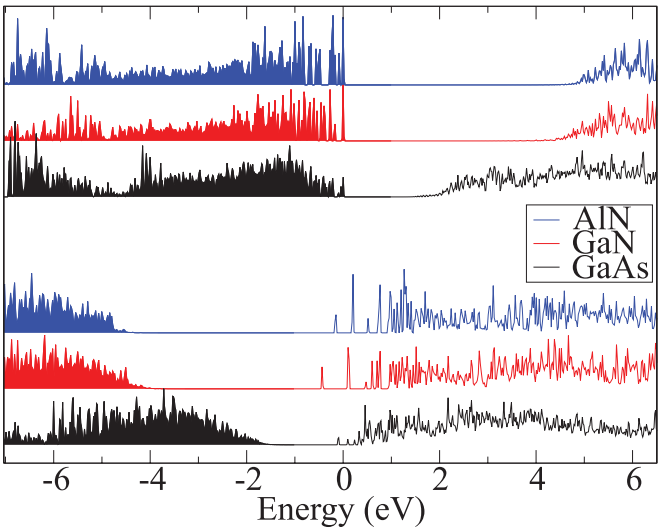

FIG. 8. (Color online) Local densities of states of the cation-rich (top three data sets) and anion-rich (bottom three data sets) polar surfaces of AlN, GaN, and GaAs. For ease of comparison, we have shifted the energy of the highest occupied state of each rod to zero.

which is positively correlated with the bulk semiconductor band gap. The nanorod of the largest band-gap semiconductor, AlN, supports the largest polarization, and the nanorod with the lowest, GaAs, supports the smallest. However, ΔV is not equal to, or proportional to, the bulk band gap. This is due to two factors: first, the effect of quantum confinement, described in Sec. V, increases the band gap by an amount that varies depending on the type of material; and second, the polar surface states responsible for pinning the Fermi level, particularly on the bottom surface of the rod, can be seen in Fig. 8 to lie at different positions relative to the local band edges in all three rods.

The amount of excess charge on the bottom ends of the rods Q_b is also positively correlated with the semiconductor band gap. However, it is not proportional to d_z, so there must be a significant difference in how this charge is distributed along the rods. We measure the decay rate of the long-range tails of excess charge, which can be seen in the magnified plot in Fig. 7. Nanorods of higher band-gap materials exhibit a larger decay constant (Table I), and therefore, stronger localization of their excess surface charges. This stronger localization is indicative of the fact that rods of lower-permittivity materials more strongly concentrate the field lines associated with surface charge, and therefore exhibit a weaker long-range decay of their internal electric fields for a given finite cross-sectional area. Therefore, rods of lower- permittivity materials require less excess charge density on their ends to attain a particular potential difference ΔV (and polarization) than do rods of higher-permittivity materials. This is a similar argument to the one in Sec. V, which also concluded that rods exhibiting weaker decay of their internal fields (i.e., thick rods), require less excess surface charge density to attain a particular ΔV. This effect can be partially incorporated in our model in Sec. V, by introducing a material-dependent constant of proportionality that determines the effective cross-sectional area seen by the electrons for a given geometrical cross-sectional area. This effective cross-sectional area is larger in materials of lower permittivity.

VII. SUMMARY AND CONCLUSION

The potential difference across a nanorod due to its large dipole moment shows up in the LDOS as a shifting of the energy of the states as one moves along the length of the rod. In this work and in our previous work,[17] it has been found that nanorods of a variety of surface terminations have Fermi levels that coincide with a high LDOS at their polar end surfaces. These are either mid-gap states or states close to the band edges. In the latter case, this means that the potential difference across the rod is approximately equal to its local band gap.

These are very stable positions for the Fermi level because small deviations from these energies result in changes in occupancy and a redistribution of charge, which generates a potential that opposes the initial change. This phenomenon is a generalization of the FLP effect on semi-infinite surfaces to structures of small dimensions.

In this work, we provide evidence that FLP plays a determining role for the polarity of nanorods. Pinning of the Fermi level results in a pinning of the potential difference ΔV across the nanorod, and hence its dipole moment.

We demonstrate that simple ionic or bond-electron counting models can be inadequate for describing, even qualitatively, differences in polarity between nanorods of different surface termination. In particular, we have shown that the effect of varying the ionic charge on the ends of a rod can be screened out, due to pinning at the nanorod ends, so as to maintain the nanorod's polarity.

We show that FLP can play a determining role in the scaling of the dipole moment with nanorod size. It is also able to account for differences in polarity between nanorods of different composition.

A particularly striking consequence of this effect is that it implies a crucial role for the solvent in determining the properties of a nanorod. Not only does the choice of solvent determine whether charge can be transferred between the ends of the nanorod, because it mediates this transfer, but it can also alter the LDOS on the nanorod ends by changing the surface chemistry. We propose that this latter effect, coupled with FLP, could have a dramatic effect on the dipole moment, and hence the optical properties.

Clearly, the picture discussed in this work could have important consequences for the response properties of nanorods in applied electric fields, and in the fields of neighboring polar nanorods. This could be important, not only for their optical properties, but also for the energetics of self-assembly of polar semiconductor nanostructures.

ACKNOWLEDGMENTS

This work was supported by EPSRC (UK) under Grant No. EP/G05567X/1, the EC under Contract No. MIRG-CT-2007-208858, and a Royal Society University Research Fellowship (P.D.H.). All calculations were run on the Imperial College HPC Service.

*p.haynes@imperial.ac.uk

[1] M. A. El-Sayed, Acc. Chem. Res. **37**, 326 (2004).

[2] X. Michalet, F. F. Pinaud, L. A. Bentolila, J. M. Tsay, S. Doose, J. J. Li, G. Sundaresan, A. M. Wu, S. S. Gambhir, and S. Weiss, Science **307**, 538 (2005).

[3] N. Tessler, V. Medvedev, M. Kazes, S. Kan, and U. Banin, Science **295**, 1506 (2002).

[4] M. Kazes, D. Y. Lewis, Y. Ebenstein, T. Mokari, and U. Banin, Adv. Mater. **14**, 317 (2002).

[5] W. U. Huynh, J. J. Dittmer, and A. P. Alivisatos, Science **295**, 2425 (2002).

[6] Z. Nie, A. Petukhova, and E. Kumacheva, Nature Nanotechnol. **5**, 15 (2010).

[7] E. V. Shevchenko, D. V. Talapin, N. A. Kotov, S. O'Brien, and C. B. Murray, Nature (London) **439**, 55 (2006).

[8] S. A. Blanton, R. L. Leheny, M. A. Hines, and P. Guyot-Sionnest, Phys. Rev. Lett. **79**, 865 (1997).

[9] M. Shim and P. Guyot-Sionnest, J. Chem. Phys. **111**, 6955 (1999).

[10] L.-S. Li and A. P. Alivisatos, Phys. Rev. Lett. **90**, 097402 (2003).

[11] D. V. Talapin, E. V. Shevchenko, C. B. Murray, A. V. Titov, and P. Král, Nano Lett. **7**, 1213 (2007).

[12] J. Goniakowski, F. Finocchi, and C. Noguera, Rep. Prog. Phys. **71**, 016501 (2008).

[13] E. Rabani, B. Hetényi, B. J. Berne, and L. E. Brus, J. Chem. Phys. **110**, 5355 (1999).

[14] E. Rabani, J. Chem. Phys. **115**, 1493 (2001).

[15] S. Shanbhag and N. A. Kotov, J. Phys. Chem. B **110**, 12211 (2006).

[16] S. Dag, S. Wang, and L.-W. Wang, Nano Lett. **11**, 2348 (2011).

[17] P. W. Avraam, N. D. M. Hine, P. Tangney, and P. D. Haynes, Phys. Rev. B **83**, 241402 (2011).

[18] C.-K. Skylaris, P. D. Haynes, A. A. Mostofi, and M. C. Payne, J. Chem. Phys. **122**, 084119 (2005).

[19] N. D. M. Hine, M. Robinson, P. D. Haynes, C.-K. Skylaris, M. C. Payne, and A. A. Mostofi, Phys. Rev. B **83**, 195102 (2011).

[20] C.-K. Skylaris and P. D. Haynes, J. Chem. Phys. **127**, 164712 (2007).

[21] C.-K. Skylaris, P. D. Haynes, A. A. Mostofi, and M. C. Payne, J. Phys. Condens. Matter **17**, 5757 (2005).

[22] C. A. Rozzi, D. Varsano, A. Marini, E. K. U. Gross, and A. Rubio, Phys. Rev. B **73**, 205119 (2006).

[23] N. D. M. Hine, J. Dziedzic, P. D. Haynes, and C.-K. Skylaris, J. Chem. Phys. **135**, 204103 (2011).

[24] P. D. Haynes, C.-K. Skylaris, A. A. Mostofi, and M. C. Payne, Chem. Phys. Lett. **422**, 345 (2006).

[25] A. Qteish and R. J. Needs, Phys. Rev. B **43**, 4229 (1991).

[26] S. G. Louie, S. Froyen, and M. L. Cohen, Phys. Rev. B **26**, 1738 (1982).

[27] S. J. Clark, M. D. Segall, C. J. Pickard, P. J. Hasnip, M. I. J. Probert, K. Refson, and M. C. Payne, Z. Kristallogr. **220**, 567 (2005).

[28] X. Huang, E. Lindgren, and J. R. Chelikowsky, Phys. Rev. B **71**, 165328 (2005).

[29] H. Yamashita, K. Fukui, S. Misawa, and S. Yoshida, J. Appl. Phys. **50**, 896 (1979).

[30] D. Brunner, H. Angerer, E. Bustarret, F. Freudenberg, R. Hopler, R. Dimitrov, O. Ambacher, and M. Stutzmann, J. Appl. Phys. **82**, 5090 (1997).

[31] Y. Goldberg, in *Properties of Advanced Semiconductor Materials GaN, AlN, InN, BN, SiC, SiGe*, edited by M. E. Levinshtein, S. L. Rumyantsev, and M. S. Shur (John Wiley & Sons, New York, 2001), pp. 31–47.

[32] H. Teisseyre, P. Perlin, T. Suski, I. Grzegory, S. Porowski, J. Jun, A. Pietraszko, and T. D. Moustakas, J. Appl. Phys. **76**, 2429 (1994).

[33] I. Vurgaftman and J. R. Meyer, J. Appl. Phys. **94**, 3675 (2003).

[34] V. Bougrov, M. E. Levinshtein, S. L. Rumyantsev, and A. Zubrilov, in *Properties of Advanced Semiconductor Materials GaN, AlN, InN, BN, SiC, SiGe*, edited by M. E. Levinshtein, S. L. Rumyantsev, and M. S. Shur (John Wiley & Sons, New York, 2001), pp. 1–30.

[35] H. C. Casey, D. D. Sell, and K. W. Wecht, J. Appl. Phys. **46**, 250 (1975).

[36] S. Adachi, J. Appl. Phys. **53**, 8775 (1982).